NASA TM X-67924

NASA TECHNICAL MEMORANDUM

NASA TM X-67924

EFFECT OF BUOYANCY ON FUEL CONTAINMENT IN AN OPEN-CYCLE GAS-CORE NUCLEAR ROCKET ENGINE

by Henry A. Putre
Lewis Research Center
Cleveland, Ohio

TECHNICAL PAPER proposed for presentation at Second Symposium on Uranium Plasma sponsored by the American Institute of Aeronautics and Astronautics
Atlanta, Georgia, November 15-19, 1971

EFFECT OF BUOYANCY ON FUEL CONTAINMENT IN AN OPEN-CYCLE GAS-CORE NUCLEAR ROCKET ENGINE

by Henry A. Putre
National Aeronautics and Space Administration
Lewis Research Center
Cleveland, Ohio

Abstract

In the latest open-cycle gas-core concept, the large fuel-to-propellant density ratio of 10 or more, coupled with a vehicle acceleration of approximately 0.02 "g" would cause a buoyancy force which would tend to reduce the amount of fuel contained in the cavity. This effect of buoyancy on fuel containment would depend on various engine flow parameters. It is not clear how these parameters interact. Experimental flow tests covering a sufficiently wide range of parameters would be too costly.

The purpose of this analysis is to determine scaling laws for the buoyancy effect so that experimental conditions can be related to the engine conditions. The fuel volume fraction (proportional to the contained fuel mass) in a short coaxial flow cavity is calculated with a programmed numerical solution of the steady Navier-Stokes equations for isothermal, variable density fluid mixing. The solution includes buoyancy, pressure gradient, and viscous shear terms, as well as the effects of side and end walls. Solutions are obtained at a propellant-to-fuel flow ratio of 50 and a Reynolds number of 1000, for fuel-to-propellant density ratios ranging from 1.0 to 10, and for various vehicle accelerations. The main limitation of the analysis is that the numerical solution fails to converge for Reynolds numbers above about 1000.

A dimensionless parameter B called the Buoyancy number was found to correlate the fuel volume fraction for large accelerations and various density ratios. This parameter has the value $B = 0$ for zero acceleration, and $B = 350$ for typical engine conditions. Calculation results show that for B less than 5.0 the fuel volume fraction, which depends strongly on density ratio, is independent of acceleration. However, for B greater than about 40, the fuel volume fraction is nearly independent of density ratio and decreases with increasing Buoyancy number. At a particular engine value of $B = 350$ the contained fuel mass is decreased by a factor of about 4.0 due to vehicle acceleration.

Introduction

The gas-core nuclear rocket is a proposed space propulsion system capable of high specific impulse (1500 to 5000 sec) and a wide range of thrust. In the latest open cycle concept, described by Ragsdale[1], shown in Fig. 1, the heavy uranium fuel vapor fills the central region of an approximately spherical cavity and is surrounded by lighter, faster moving hydrogen propellant. The propellant stream is heated to about 20,000° K by thermal radiation from the fissioning fuel core which is at a temperature of about 60,000° K.

One characteristic of any open-cycle concept is that some unfissioned fuel is lost. This occurs because the two gases are in direct contact inside the reactor cavity. Numerous fluid mechanics studies, most of which have been experimental, have been conducted to find the flow conditions that minimize fuel loss rates and maximize the contained fuel mass (or equivalently the fuel volume fraction). Most recently the experimental work of Bennet and Johnson[2] has shown that fuel volume fractions of 30 percent at propellant-to-fuel mass flow ratios above 50 can be obtained in coaxial flow cavities.

The recent emphasis on relatively low thrust, very high specific impulse, engines for Mars missions[1] calls for engine flow conditions with very low average fuel velocities (about 0.01 ft/sec), and a fuel density that is about ten to twenty times the average propellant density. Vehicle acceleration would be approximately 0.02 times earth gravity. These flow conditions can lead to large buoyancy forces on the fuel with the result that fuel containment may be reduced by fuel acceleration out of the cavity. Such a "buoyancy effect" was observed experimentally by Bennet and Johnson[2] in a two-fluid coaxial flow cavity. Although it was not a strong effect in the experiment, these investigators concluded that at conditions close to the engine the effect could be much stronger because the fuel velocities in the engine are much less than in the experiment.

The effect of buoyancy on fuel containment would depend on many engine parameters, such as inlet velocity and density, cavity geometry, Reynolds number, and vehicle acceleration. It is not clear how these parameters interact. A thorough experimental study covering the full range of parameters would be much too costly, if not impossible. Therefore analytical predictions are needed to generalize the experimental results so that one can extrapolate the present observations to the engine conditions. This report describes an analysis that determines the functional dependence of contained fuel mass (or fuel volume fraction) on the fuel-to-propellant density ratio and vehicle acceleration for the simplified case of isothermal flow in a short cylindrical cavity.

The purpose of this report is to analytically determine the proper scaling laws for the "buoyancy effect" so that experimental conditions can be related to engine conditions. Previous analyses such as for the ducted jet by Ghia[3], the free jet by Putre[4] or the steady Navier-Stokes equation solution of the ducted jet by Shavit[5] were ruled out for this study, either because the equation sets used neglected pressure gradients and recirculating flows, or because the influence of the end walls (i.e., the nozzle constriction) was not included. It was felt that these factors might be important elements of the buoyancy effect. The main assumption of the present analysis is that the flow is steady, isothermal, and laminar. The analysis includes a complete fluid force balance, including pressure terms, viscous shear terms, buoyancy terms, and effects due to a downstream end wall.

The number of parametric calculations is nec-

essarily limited because of the relatively long computing times for the numerical solution (typically 15 minutes per case), which was due mainly to numerical convergence requirements. Therefore, the following quantities were fixed as shown in Fig. 2: cavity L/D = 1, propellant-to-fuel mass flow ratio of 50, Reynolds number of 1000, and nozzle area ratio of 4 to 1. The generalized inlet velocity and fuel concentration profiles are also fixed. The fuel-to-propellant density ratio is varied from 1.0 to 10.0 (and similarly the velocity ratio). As will be described in subsequent sections of this report, the buoyancy force can be characterized by a dimensionless Buoyancy number, B, which is proportional to the square root of vehicle acceleration. The B value in the calculations will be varied from zero to the largest value for which the program converges, or about B = 100. The computed results will be extrapolated to B values near 350, which correspond to the "0.02 g" level of the engine. As is shown in Fig. 2, except for Reynolds number, these flow conditions compare closely to the experimental conditions of Ref. 2, so that the results of this study can be applied to the coaxial flow experiment.

Symbol List

a,b,c,d	generalized coefficients in the three flow equations
$\bar{a},\bar{b}$	generalized coefficients in the substitution equations
B	Buoyancy number, defined in equation (15)
D	cavity diameter
F	generalized dependent flow variable in the three flow equations
f(r)	smoothing function for inlet velocity and mass fraction profile
g	vehicle acceleration
L	length of cavity
m	mass flow rate
n	normal distance from wall
R	cavity radius
Re	Reynolds number = $\frac{2(m_P + m_F)}{\pi R \mu}$
RU1,RU2	inner and outer velocity buffer radius
RY1,RY2	inner and outer mass fraction buffer radius
r	radial co-ordinate
Sc	Schmidt number
U	specified axial velocity at the inlet
u	axial velocity
VF	fuel volume fraction, defined as the fraction of the cavity filled with pure fuel if it were gathered together into a central volume
v	radial velocity
x	axial coordinate
y	fuel mass fraction, local fuel density/ local mixture density
ρ	density
μ	viscosity
ω	vorticity
ψ	stream function
φ	generalized dependent flow variable in the substitution equations

Subscripts:

F	fuel
i	index for central node
j,e,w,n,s	indices for surrounding nodes
K	index for each of three flow equations
P	propellant
0,1	wall node, adjacent inside node

Analysis

The cavity flow model to be analyzed is shown in Fig. 3. The analysis is restricted to a rectangular cylinder geometry as shown. The assumptions of the analysis are:

1. Steady, viscous flow, constant viscosity
2. Isothermal flow
3. Inlet and outlet flows are purely axial
4. Impermeable, no-slip side and end walls

Equation Set

The system of equations to be solved is a rewritten form of the variable density Navier-Stokes equations, the continuity equation, and the mass diffusion equation. The solution method is basically the same one described in detail by Gosman, et al.[6]. For sake of brevity only the main points of the analysis are repeated here. The rewritten equation set takes the form of three simultaneous, and similar, second order nonlinear partial differential equations in the variables vorticity, stream function, and fuel mass fraction (concentration). These equations are generalized into the form

$$a_K\left\{\frac{\partial}{\partial x}\left(F_K\frac{\partial\psi}{\partial r}\right) - \frac{\partial}{\partial r}\left(F_K\frac{\partial\psi}{\partial x}\right)\right\} - \frac{\partial}{\partial x}\left\{b_K\, r\frac{\partial}{\partial r}(c_K F_K)\right\} - \frac{\partial}{\partial r}\left\{b_K\, r\frac{\partial}{\partial r}(c_K F_K)\right\} + r\, d_K = 0 \qquad (K = 1,2,3) \qquad (1a,b,c)$$

The first line in this general equation has the convective terms, the second line has the diffusive terms, and the third line has the general source term including the acceleration body force term. The coefficients a_K, b_K, c_K, and d_K can depend on

x,r and the primary variable F_K, and are given in table I. The Schmidt number is taken as Sc = 1.51.

The value of axial acceleration g in the body force term of d_1 (see table I) is specified in terms of the dimensionless Buoyancy number

$$B = \sqrt{\frac{(\rho_F - \rho_P)gD}{\rho_F U_F^2}}$$

where the form of B is discussed later.

Additional equations are for vorticity and stream function in terms of velocities, and for density in terms of mass fraction.

$$u = \frac{1}{\rho r}\frac{\partial \psi}{\partial r} \tag{2}$$

$$v = -\frac{1}{\rho r}\frac{\partial \psi}{\partial x} \tag{3}$$

$$\omega = \left(\frac{\partial v}{\partial x} - \frac{\partial u}{\partial r}\right) \tag{4}$$

$$\rho = \frac{\rho_F \rho_P}{\rho_F + y(\rho_P - \rho_F)} \tag{5}$$

The solution of this equation set requires that the values of F_K or $\partial F_K/\partial n$ be specified on all boundaries of the flow region. The centerline boundary conditions are:

$$\frac{\partial}{\partial r}\left(\frac{\omega}{r}\right) = 0,\ \psi = 0,\ \frac{\partial y}{\partial r} = 0;\ \text{at}\ \ r = 0 \tag{6}$$

The outer no-flow wall boundary conditions are:

$$\psi = \text{const},\ \left(\frac{\omega}{r}\right)_0 = \left[\frac{3(\psi_1 - \psi_0)}{r_0^2 n_1^2 \rho} + \frac{1}{2}\left(\frac{\omega}{r}\right)_1\right],\ \frac{\partial y}{\partial n} = 0 \tag{7}$$

where the wall and inside node are given the subscripts 0 and 1, respectively. The outlet boundary conditions are, for the outlet far from the corner:

$$\frac{\partial\left(\frac{\omega}{r}\right)}{\partial x} = 0,\ \frac{\partial \psi}{\partial x} = 0,\ \frac{\partial y}{\partial x} = 0 \tag{8}$$

The boundary conditions of Eqs. (6) to (8) are quite general in that the same equations apply for any flow in the cavity. On the other hand the flow is strongly influenced by the inlet boundary conditions. Therefore, these were chosen to resemble the inlet conditions in the experiment of Ref. 2. The inlet velocity profiles and mass fraction profiles were specified as smooth profiles with buffer regions (see fig. 3) and were numerically integrated to get the inlet stream function values. These are specified in the forms

$$r < RY1,\ y = 1.0;\ RY1 \le r \le RY2,\ y = 1 - f(r),$$
$$r > RY2,\ y = 0 \tag{9}$$

$$r < RU1,\ u = U_F;\ RU1 \le r \le RU2,$$
$$u = U_F + (U_P - U_F)f(r),\ r > RU2,\ u = U_P \tag{10}$$

$$\psi(x = 0) = \int_0^r \rho u r\, dr \tag{11}$$

where f(r) is a double parabola smoothing function that runs from 0 to 1. Based on preliminary calculations, the buffer radii values were chosen as RY1 = 7/21, RY2 = 11/21, RU1 = 10/21, RU2 = 18/21.

Realistic vorticity inlet conditions that are compatible with the above inlet conditions must also be specified. The inlet vorticity is related to the "straightness" of the inlet flow through Eqs. (2) to (4). The inlet vorticity was calculated from the expanded equation

$$\frac{\omega}{r}(x = 0) = -\frac{1}{r}\left[\frac{1}{\rho r}\frac{\partial^2 \psi}{\partial x^2} + \frac{1}{r}\frac{\partial \psi}{\partial x}\frac{\partial}{\partial x}\left(\frac{1}{\rho}\right) + \frac{\partial u}{\partial r}\right] \tag{12}$$

where the term with $\partial\psi/\partial x$ is identically set to 0 to represent a purely coaxial flow at the inlet. As will be discussed later, the inlet conditions are completely specified when RU1, RU2, RY1, RY2, ρ_F, U_F, ρ_P, and U_P are specified.

The fuel volume fraction is defined to be the fraction of the cavity filled with pure fuel if it were gathered together into a central volume. This quantity is calculated from

$$VF = \frac{2}{\rho_F R^2 L}\int_0^L \int_0^R y\rho r\, dr\, dx \tag{13}$$

Numerical Solution Method

The numerical solution is based on the method detailed in Ref. 6. In simple terms, the Eqs. (1a, b,c) are written in terms of finite differences at node points of a rectangular mesh covering the flow region. Central differences are used for all terms except the convective terms which use upwind differences. (Upwind differencing improves the stability of the numerical solution.) The resulting equation set can be written in the form

$$\varphi_i = \sum_{j=e,w,n,s} (\bar{a}_{ij}\varphi_j + \bar{b}_i) \tag{14}$$

where φ_i is one of the primary variables ω/r, ψ or y. And a_{ij} or b_i may depend on φ_i.

The upwind differences make the coefficient matrix of this equation set diagonally dominant. Thus if the coefficients a_{ij} and b_i were constants (linear equation), the solution by successive substitution (also known as Gauss Seidel iteration) would be absolutely convergent. These coefficients will depend on local gradients, especially velocity and density gradients. Hence, convergence may be difficult for those cases with very large gradients.

The stability of the equations (tendency to converge) were further improved by several methods. First, the buffer regions in the inlet velocity and fuel concentration profiles were made as large as possible to reduce the gradients at the inlet. Secondly, the mesh was stretched in the x direction with node points closer at the inlet than at the outlet. Thirdly, underrelaxation was used to dampen fluctuations in the coefficients between

iterations. After extensive trial runs it was found that, for convergence over the large range of density ratios and velocity ratios to be studied, the stream function, local density, and vorticity source term d_K, required underrelaxation.

Computer Program

The numerical solution was programmed for use on the IBM 7090/94 computer. The program was based on the basic code described in Gosman, et al.[6]. Substantial modifications and additions were made to this basic code. These included a subroutine for specifying and integrating the inlet velocity, mass fraction, and stream function profiles; a subroutine for calculating the source term (d_K), including the gravity term for the vorticity equation; a boundary condition subroutine; a velocity and density distribution subroutine; as well as input-output routines such as for writing tapes to restart calculations and to generate microfilm contour plots of stream function and fuel mass fraction.

Calculations were usually initialized by starting from a previous solution on tape. This method reduced computing time by factors of 2 or 3. The iterations were run until the change in F_K between successive iterations was less than 0.1 percent. A typical case calculation with a 22 x 25 mesh required about 300 iterations with about 15 minutes of computing time.

Results and Discussion

The results of preliminary runs for determining the range of input parameters for convergence, and the selection of inlet conditions are discussed first. Then the results of parametric runs at various density ratios and vehicle accelerations are discussed and analyzed.

Limits on Range of Input Parameters for Convergence

As was discussed in the Analysis section, the numerical solution fails to converge when the equations become strongly nonlinear because of large gradients in the flow variables. The conditions for improved stability given in the Analysis section were used to obtain convergence for a fairly large range of parameters. Trial runs showed that the smallest flow ratios gave convergence at the highest Reynolds numbers. Thus, for this report the flow ratio was fixed at the smallest realistic value of propellant-to-fuel-flow ratio of 50. This gave convergence to Reynolds number as large as 10,000 with a density ratio of unity. For the parametric calculations using fuel-to-propellant density ratios from 1.0 to 10.0, a constant Reynolds number of 1000 was used to assure convergence. The runs for various buoyancy forces failed to converge for Buoyancy numbers, B, greater than 100.

Effect of Inlet Conditions

Preliminary runs showed that for a fixed flow ratio and density ratio the cavity flow is strongly dependent on the inlet velocity and concentration profiles. The object of these preliminary runs was to determine those buffer radii for Eqs. (8) to (10) which resulted in the largest fuel volume fraction with good convergence. It was found that step profiles resulted in strongest recirculation and low fuel volume fractions. Profiles with wide buffer layers resulted in least recirculation and increased fuel volume fractions. (In general strong recirculation coincided with low fuel volume fractions.) The buffer radii values which resulted in the largest fuel volume fraction values for fuel-to-propellant density ratios of 1.0 to 2.0, are given in the Analysis section. (These buffer radii were not re-optimized for other density ratios, or for the nonzero buoyancy force cases.) It is worth noting that these analytically determined buffer values give about the same optimum inlet profiles as were experimentally determined by Johnson[2].

Streamline and Fuel Concentration Plots

The effect of various density ratios and vehicle accelerations on the general cavity flow is best illustrated by the streamline and fuel concentration contour plots in Figs. 4 to 6. These figures are from computer plots of the converged numerical solutions. The streamline plots in Fig. 4 and the fuel mass fraction contour plots in Fig. 5 show the large recirculation cell that is formed when the density ratio is increased from $\rho_F/\rho_P = 1.0$ to 4.0 with no buoyancy force. This recirculation cell, clearly outlined by the zero streamline in Fig. 4(b), convects a substantial amount of fuel away from the fuel plume, thus reducing the fuel mass in the cavity. This explains the reverse curvature of the 50 percent contour in Fig. 5(b) as compared to Fig. 5(a). The fuel volume fraction decreases from 0.072 to 0.034 as the density ratio increases from 1.0 to 4.0.

The concentration contour plots in Fig. 6 show the effect of vehicle acceleration on the shape and size of the fuel plume for a density ratio of $\rho_F/\rho_P = 2.0$. Figure 6 shows that, as vehicle acceleration increases from B = 0 to 65, the fuel plume is stretched out and gets much narrower. The fuel volume fraction decreases from 0.059 to 0.0126, by nearly a factor of five. This fuel region stretching is the result of buoyancy force accelerating the fuel toward the downstream end. The concentration contours at B values near 100 for density ratios greater than 1.0 have shapes similar to those in Fig. 6(b). These flows are characterized by an absence of the recirculating cell mentioned above (with zero acceleration), and by substantially lower fuel volume fractions.

It should be noted that the fuel volume fractions calculated for all cases of this report are factors of nearly 5 below the measured values from the coaxial flow experiments of Ref. 2. As discussed above, the specified inlet boundary conditions were optimized by preliminary runs, to give the largest calculated fuel volume fractions. Thus no significant increase in calculated fuel volume fractions is expected for different inlet conditions. Therefore it appears that the low calculated values of fuel volume fractions could possibly be the result of the calculations being limited to Reynolds numbers near 1000. This is somewhat confirmed by the fact that additional calculations for a density ratio of 1.0 at Reynolds number of 10,000 resulted in a fuel volume fraction of 0.108 compared to the value of 0.072 at the Reynolds number of 1000. The fact that the

analysis does not converge for very high Reynolds numbers, and that it results in consistently low fuel volume fractions, are the major shortcomings of this analysis. However, this investigation is concerned mainly with the functional dependence of fuel volume fraction on various parameters. Thus for purposes of this report we are not as concerned with the precise values of fuel volume fraction as with the trends in the values.

The variation of the flow with mass flow ratio and outlet diameter is also noted here. Based on a few calculations, the larger mass flow ratios, m_P/m_F, require larger values of velocity ratio, U_P/U_F, which results in stronger recirculation and correspondingly lower fuel volume fraction. The outlet diameter for the parametric runs was 0.48 times the cavity diameter. When the outlet diameter was decreased to as small as 0.14 times the cavity diameter, the fuel volume fraction for a fixed engine acceleration was not significantly changed.

Effect of Density Ratio on Fuel Volume Fraction at "Zero-g"

The flow equations were solved for fuel-to-propellant density ratios of 1.0, 2.0, 4.0, and 10.0. The flow ratio was fixed at $m_P/m_F = 50$, and the Reynolds number was 1000. The buoyancy force for these cases was assumed to be zero. The propellant to fuel flow ratio was adjusted over the range $U_P/U_F = 16.3$ to 183 to maintain the fixed flow ratio. The variation of fuel volume fraction with density ratio is shown in Fig. 7. The fuel volume fraction decreases from 0.072 to 0.017 as density ratio increases from $\rho_F/\rho_P = 1.0$ to 10.0. The fuel volume fraction first decreases slowly as density ratio increases from 1.0 to 2.0, and decreases faster (as the -3/4 power of density ratio) for density ratios beyond about 2.0. The two-region behavior is probably due to the fact that for the flow ratio of 50 recirculation starts at about $\rho_F/\rho_P = 2.0$ and becomes stronger with increasing density ratio. The -3/4 power dropoff with density ratio is stronger than was calculated in Ref. 4 with a boundary layer solution (which did not include recirculation) where the variation was as the -1/2 power. The experimental results of Ref. 2 also showed about a -1/2 power variation, which was probably due to the fact that at the high Reynolds numbers recirculation was weaker than in the present calculations.

Effect of Acceleration on Fuel Volume Fraction

Solutions of the flow equations were obtained for various fuel-to-propellant density ratios and for various vehicle accelerations. The vehicle acceleration was originally specified in terms of a Froude number, U_F^2/gD, which is the conventional measure of fuel inertia to acceleration force. Values of Froude number were varied from 10^{-5} to infinity. A simplified analysis indicated that density ratio should be included in a buoyancy parameter. Several dimensionless combinations are possible. After several different ways were used for plotting the calculated results, it was concluded that the best parameter for characterizing and generalizing the buoyancy effect has the form:

$$B = \sqrt{\frac{(\rho_F - \rho_P)gD}{\rho_F U_F^2}} \qquad (15)$$

This parameter is called the Buoyancy number in this report. The combination inside the radical is a measure of the buoyancy force to the inertia force on the fuel. The square root is used for ease in plotting the B values which range from 0 to about 350.

The fuel volume fraction is plotted in Fig. 8 as a function of Buoyancy number for various density ratios. The calculations range from B = 0 to about 100, where the upper value is the numerical convergence limit. For a fixed density ratio the fuel volume fraction is constant for small B values, and decreases as a constant power of B for large B values. Of particular importance is the fact that, for the combination of variables in B, the curves for the various density ratios fall close together at large B values, which confirms the form of Eq. (15).

At Buoyancy numbers above about 40, the fuel volume fractions are close enough to a single exponential line that they may be represented by a single correlating curve. This correlating line is shown dotted in Fig. 8 and is given by the equation

$$VF(B \geq 40) = 0.20\ B^{-2/3} \qquad (16)$$

This line is used to extrapolate the calculations to the Buoyancy number of 350 at the engine acceleration of "0.02 g." At a density ratio of 10.0, which is close to the engine value, it is seen in Fig. 8 that the fuel volume fraction is decreased due to buoyancy effect by a factor of about 4.0.

This reduction in fuel volume fraction should be investigated and verified in future flow simulation experiments. The Buoyancy number of various engine designs will probably range from about B = 100 to 500, as shown in Fig. 8. By comparison, present experiments operate at Buoyancy numbers no larger than about B = 30. Therefore, for accurate assessment of the buoyancy effect, the range of experimental Buoyancy numbers should be extended into the range of engine values.

Conclusions

A two-fluid steady Navier-Stokes equation solution has been programmed for the case of coaxial flow in a gas-core nuclear rocket cavity, including the buoyancy force due to density differences and vehicle acceleration. Solutions were obtained and fuel volume fractions were calculated for a propellant-to-fuel flow ratio of 50, a Reynolds number of 1000, in an L/D = 1 cavity. The fuel-to-propellant density ratio ranged from 1.0 to 10.0 and the vehicle acceleration was varied from zero to a value for the engine. Calculated fuel volume fractions are considerably below values measured in a coaxial flow experiment. This is probably because the numerical solution converges only for Reynolds numbers below about 1000 whereas the experiment was at a Reynolds number of 2×10^5. This report is concerned with the trends in the calculated fuel volume fraction values rather than with the exact values. The Buoyancy number determined in this report to best correlate the fuel

volume fraction with density ratio, fuel velocity, and vehicle acceleration has the form:

$$B = \sqrt{\frac{(\rho_F - \rho_p)gD}{\rho_F U_F^2}}$$

Specific conclusions of this study are:

1. At Buoyancy numbers below about 5, the fuel volume fraction depends strongly on density ratio, but is independent of vehicle acceleration.

2. At Buoyancy numbers larger than 40, the fuel volume fraction is nearly independent of density ratio, and decreases with the -2/3 power of Buoyancy number.

3. For a typical engine flow with a density ratio of 10.0 and Buoyancy number of 350, the fuel volume fraction that would exist at zero g is decreased by a factor of about 4.0 due to buoyancy effect.

4. The range of current flow experiments should be extended to higher Buoyancy numbers to verify the calculated relationship between fuel volume fraction, density ratio, fuel velocity, and Buoyancy number.

References

1. Ragsdale, R. G. and Willis, E. A., "Gas-Core Rocket Reactors - A New Look," Paper 71-641, June 1971, AIAA, Salt Lake City, Utah.

2. Bennet, J. C. and Johnson, B. V., "Experimental Study of One- and Two-Component Low-Turbulence Confined Coaxial Flows," CR-1851, NASA, Cleveland, Ohio.

3. Ghia, K. N., Torda, T. P., and Lavan, Z., "Laminar Mixing of Heterogeneous Axisymmetric Coaxial Confined Jets," CR-72480, Nov. 1968, IIT Research Inst., Chicago, Ill.

4. Putre, H. A.: "Estimates of Fuel Containment in a Gas Core Nuclear Rocket," Transactions of the A.N.S. Annual Meeting, June 1970, Los Angeles, Calif., p. 346.

5. Shavit, G. "Analytical and Experimental Investigations of Laminar Mixing of Homogeneous and Heterogeneous Jets in a Confining Tube," Ph.D. Thesis, Illinois Inst. of Technology, 1970.

6. Gosman, A. D., Pun, W. M., Runchal, A. K., Spalding, D. B., and Wolfstein, M., "Heat and Mass Transfer in Recirculating Flows," Academic Press, New York, 1969.

TABLE I. - VALUES OF THE GENERALIZED COEFFICIENTS IN EQUATION (1)

K	F_K	a_K	b_K	c_K	d_K
1	$\frac{\omega}{r}$	r^2	r^2	μ	$-r\left[\frac{\partial}{\partial x}\left(\frac{u^2+v^2}{2}\right)\frac{\partial \rho}{\partial r} - \frac{\partial}{\partial r}\left(\frac{u^2+v^2}{2}\right)\frac{\partial \rho}{\partial x} + rg\frac{\partial \rho}{\partial r}\right]$
2	ψ	0	$\frac{1}{\rho r^2}$	1	$-\frac{\omega}{r}$
3	y	1	$\frac{\mu}{Sc}$	1	0

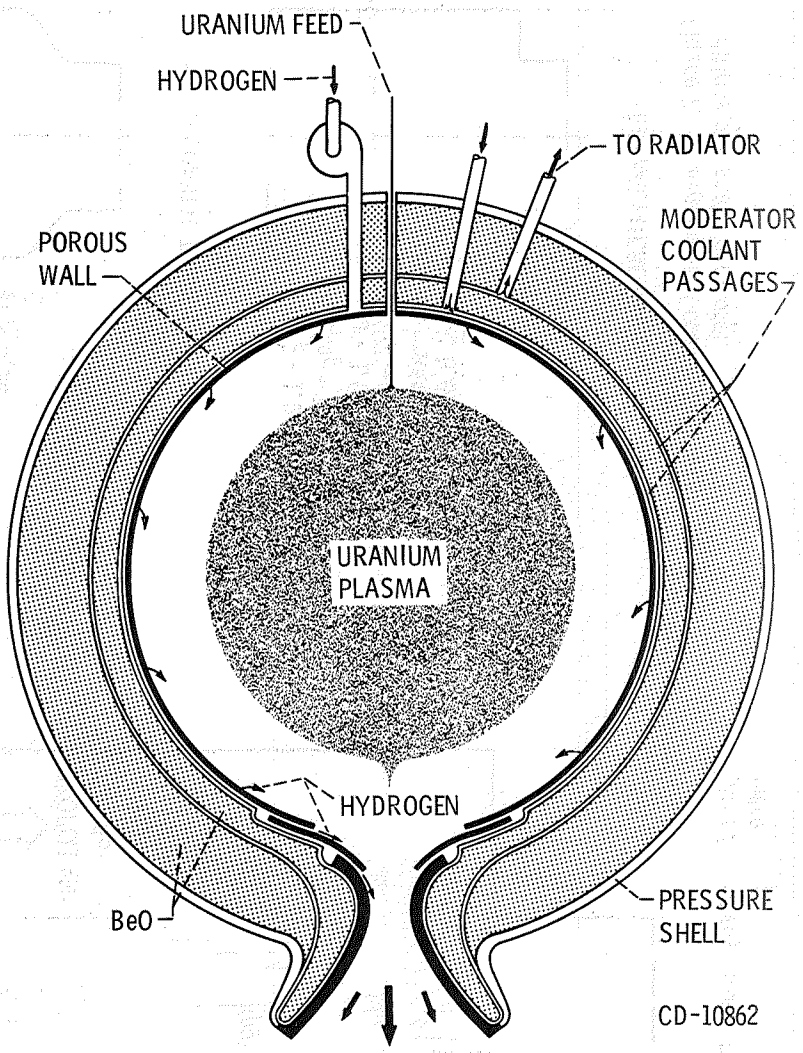

Figure 1. - Conceptual gas core nuclear rocket engine.

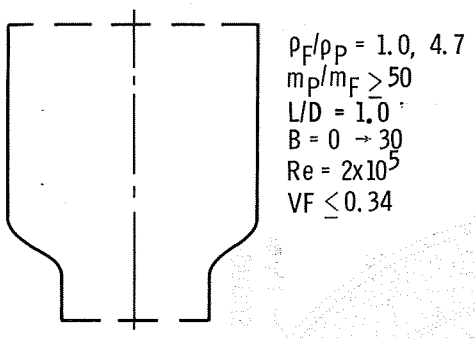

(A) COAXIAL TESTS REF. (2).

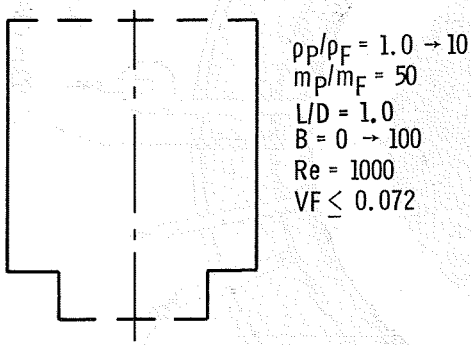

(B) ANALYTICAL MODEL.

Figure 2. - Comparison of coaxial flow conditions and analytical model.

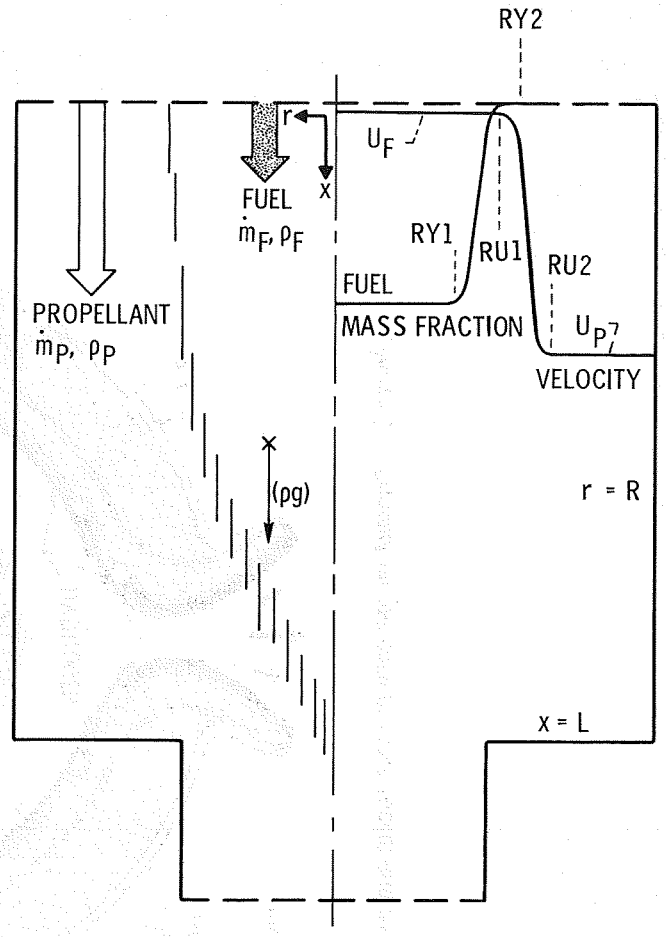

Figure 3. - Cavity model showing inlet profiles and buoyancy force.

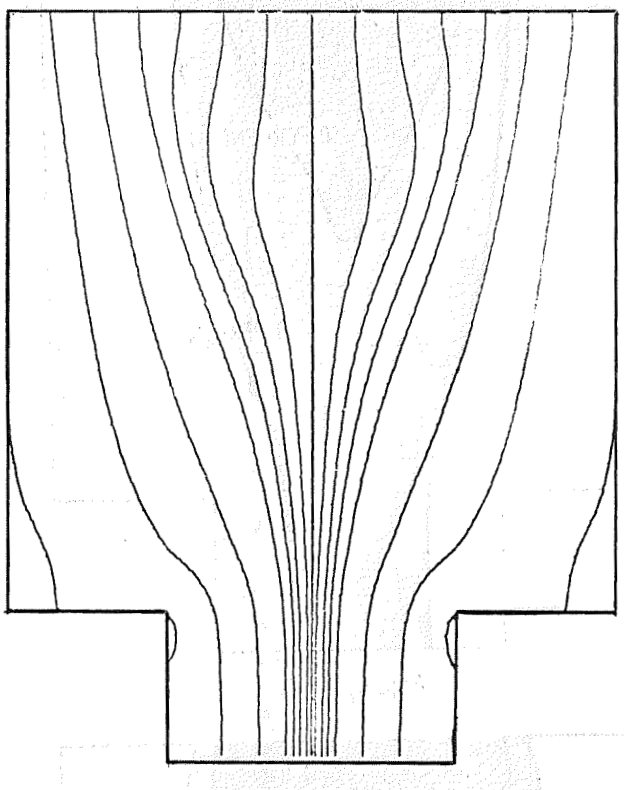

(A) $\rho_F/\rho_P = 1.0$.

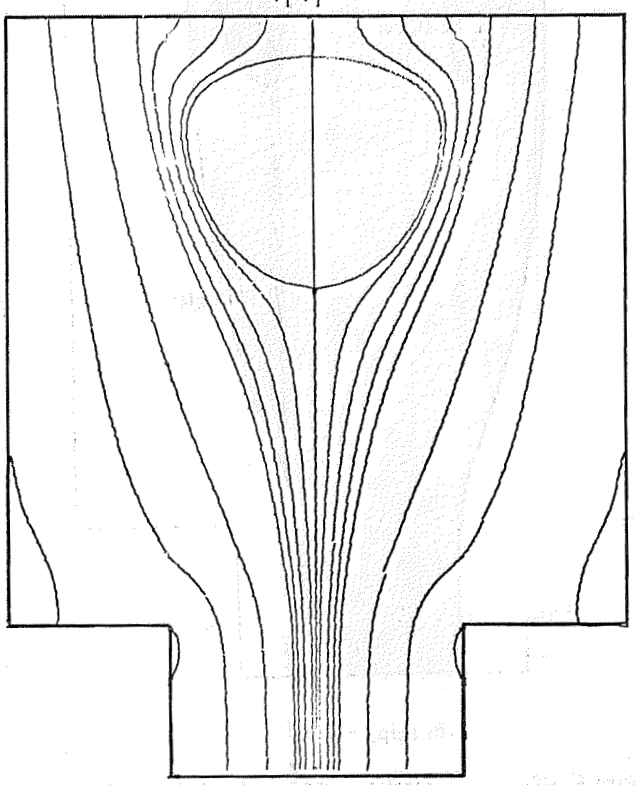

(B) $\rho_F/\rho_P = 4.0$.

Figure 4. - Streamline plots for different density ratios, $m_P/m_F = 50$, Re = 1000, B = 0.

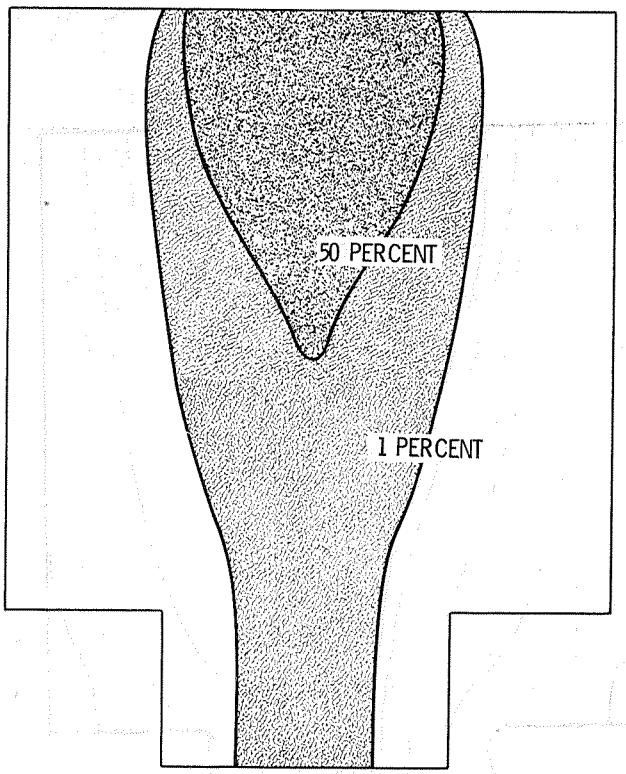

(A) $\rho_F/\rho_P = 1.0$.

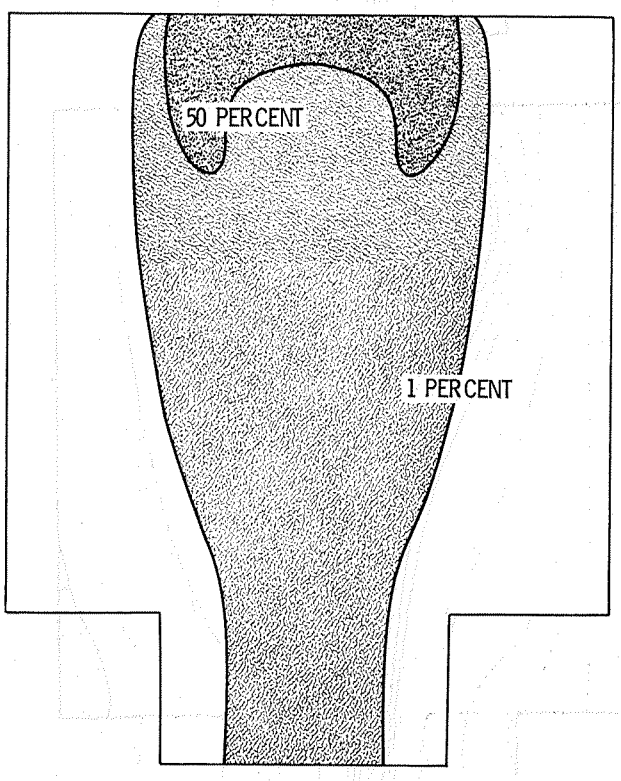

(B) $\rho_F/\rho_P = 4.0$.

Figure 5. - Fuel mass fraction contours for different density ratios, $m_P/m_F = 50$, Re = 1000, B = 0.

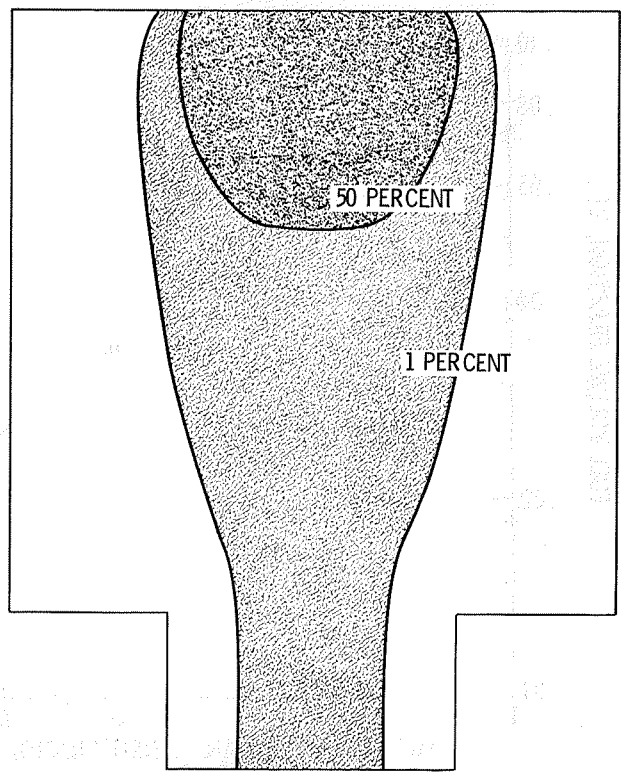

(A) B = 0.

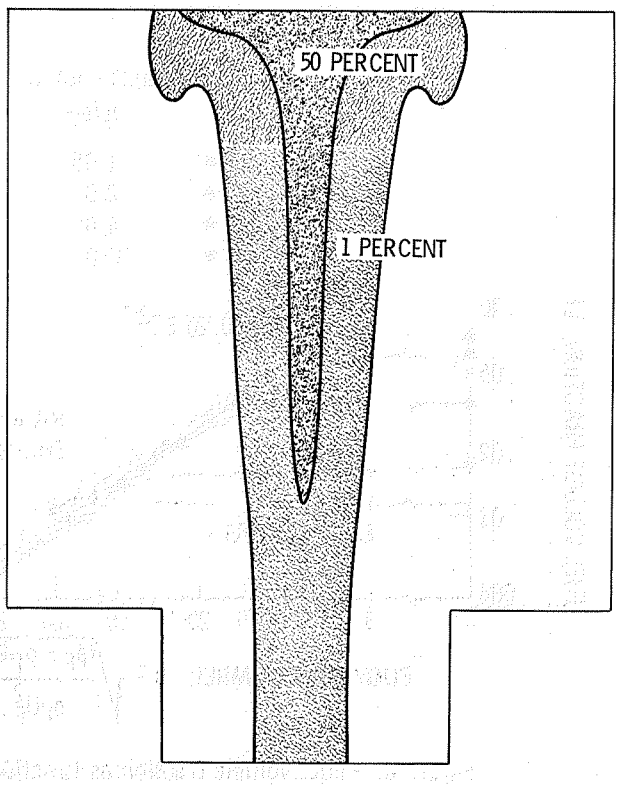

(B) B = 65.

Figure 6. - Fuel mass fraction contours for different vehicle accelerations, $m_P/m_F = 50$, Re = 1000, $\rho_F/\rho_P = 2.0$.

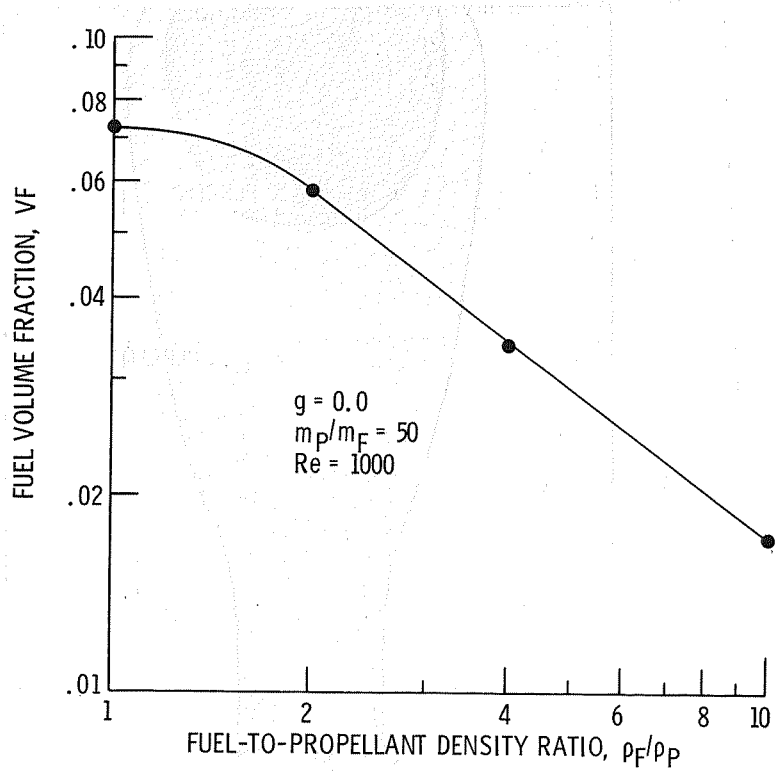

Figure 7. - Variation of fuel volume fraction with fuel-to-propellant density ratio for zero acceleration.

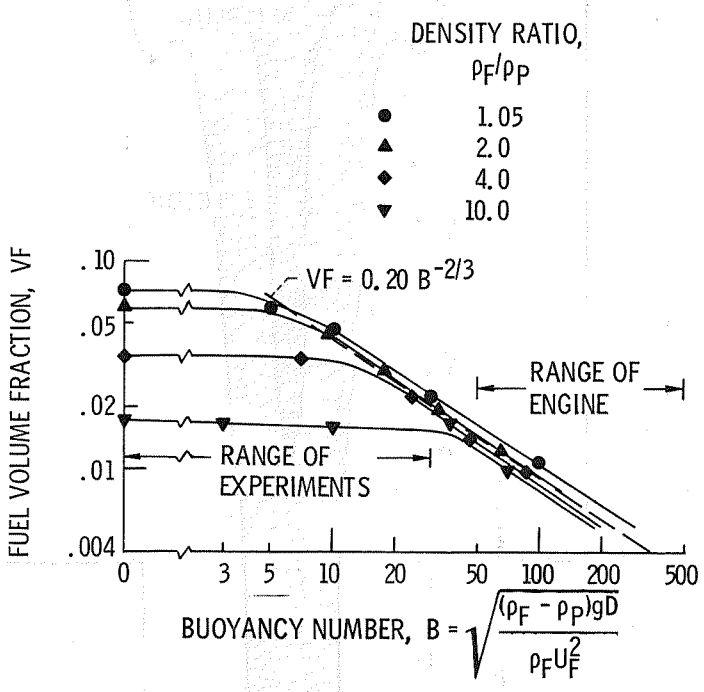

Figure 8. - Fuel volume fraction as function of buoyancy number for various density ratios. m_P/m_F = 50, Re = 1000.

NASA-Lewis-Com'l